Wrinkling reveals a new isometry of pressurized elastic shells

D. Vella[1] [(a)], H. Ebrahimi[2], A. Vaziri[2] and B. Davidovitch[3]

[1] *Mathematical Institute, University of Oxford, Woodstock Rd, Oxford, OX2 6GG, UK*
[2] *Department of Mechanical and Industrial Engineering, Northeastern University, Boston, Massachusetts 02115, USA*
[3] *Physics Department, University of Massachusetts, Amherst, Massachusetts 01003, USA*

PACS 46.32.+x – Static buckling and instability
PACS 46.70.De – Beams, plates and shells
PACS 62.20.Dc – Elasticity, elastic constants

Abstract – We consider the point indentation of a pressurized, spherical elastic shell. Previously it was shown that such shells wrinkle once the indentation reaches a threshold value. Here, we study the behaviour of this system beyond the onset of instability. We show that rather than simply approaching the classical 'mirror-buckled' shape, the wrinkled shell approaches a new, universal shape that reflects a nontrivial type of isometry. For a given indentation depth, this "asymptotic isometry", which is only made possible by wrinkling, is reached in the doubly asymptotic limit of weak pressure and vanishing shell thickness.

Introduction. – Just as one pokes an object to see how stiff it is, it is common to measure the mechanical properties of small scale objects by indentation, often using an AFM [1]. In biology and medicine many objects of interest are relatively thin capsules swollen by osmotic pressure, *e.g.* viruses [2], bacteria [3], yeast cells [4] and the polymerosomes used in drug delivery [5]. Recent studies have focussed on modelling the indentation of pressurized elastic capsules [2, 3, 5, 6] using numerous approaches including finite element methods and analytical techniques.

The problem of the indentation of a shell with no internal pressure (pressureless) has been extensively studied [8–11]. In this case, the classical picture is that a spherical shell of thickness t and radius R will accommodate indentation by 'mirror-buckling': it is as if a portion of the shell were sliced off, inverted and then reattached to the remainder of the shell (fig. 1a). In reality, the apparent discontinuity in slope is resolved by a boundary layer of width $(tR)^{1/2}$ [10]. Since mirror-buckling represents a simple isometry of the shell (i.e. there is no strain except at isolated points or along curves), the energy of deformation is localized within this boundary layer and vanishes in the limit $t \to 0$. This simple geometrical picture has recently been shown to hold even in the presence of an internal pressure, p, albeit under the assumption that the shell remains very close to an axisymmetric shape [6].

However, it is well known that deformed shells often do not remain perfectly axisymmetric. Under point indentation, pressureless shells develop vertices [12–16] while pressurized shells wrinkle (fig. 1b) [7]. A similar phenomenology is observed in other deformation modes including the contact between a plate and a shell [11, 17] and the secondary buckling of depressurized shells [18, 19].

As was shown in previous work [7], the appearance of

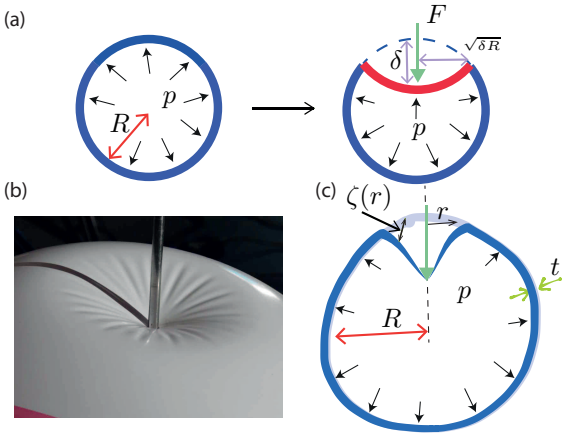

Fig. 1: (a) Schematic illustration of the mirror buckling of a pressurized shell: an indentation depth δ is accommodated by the (energetically cheap) formation of an inverted cap of width $(\delta R)^{1/2}$. (b) In reality, an indented pressurized shell wrinkles [7]. (c) Setup and notation for the model calculation of point indention of a pressurized spherical shell presented here.

(a) E-mail:dominic.vella@maths.ox.ac.uk

wrinkles upon the point indentation of a pressurized shell is indicative of azimuthal compression. Since the mirror-buckled shape remains an isometry of the shell, it is tempting to assume that the wrinkled shape will be a small perturbation of this shape, as has been proposed previously [7]. However, here we show that wrinkling changes the shape of the shell markedly. Our analysis reveals a new wrinkly isometry of the shell that is energetically cheaper than mirror buckling.

Numerical experiments. – Numerical simulations were performed using the commercial finite element package ABAQUS (SIMULIA, Providence, RI) for a spherical shell of radius $R = 1$ m, thickness in the range $0.3\text{ mm} \leq t \leq 2$ mm, Young's modulus $E = 70$ GPa, and Poisson ratio $\nu = 0.3$. The shell is subject to an internal pressure $p = O(10^5\text{ Pa})$. (Four-node thin shell elements with reduced integration were used in all calculations and a mesh sensitivity study was carried out to ensure that the results are minimally sensitive to the element size. No initial geometrical imperfection was used and the ABAQUS automatic stabilization scheme, with a dissipated energy fraction of 2×10^{-4} and an adaptive stabilization ratio of 0.05, was employed to capture instabilities in the shell.)

Simulations show that for sufficiently small indentation depths δ, the shell remains perfectly axisymmetric. In this limit the (thickness integrated) in-plane stress [11] is close to the isotropic tension prior to indentation: $\sigma_\infty = pR/2$. Deformation of the shell is resisted by a normal force that is proportional to the vertical displacement — effectively a Winkler foundation of stiffness κ_w [6]. This foundation stiffness depends on the stretching stiffness of the shell, Et, and so on dimensional grounds we might expect that $\kappa_w \sim Et/R^2$; an analysis of the governing equations confirms this expectation [6, 8]. By analogy with a liquid's meniscus, the combination of an intrinsic tension, $\sigma_\infty \sim pR$, and a linear foundation stiffness, $\kappa_w \sim Et/R^2$, gives rise to a characteristic horizontal length over which vertical deflections decay

$$\ell_p = \left(\frac{\sigma_\infty}{\kappa_w}\right)^{1/2} = \left(\frac{pR^3}{Et}\right)^{1/2}. \qquad (1)$$

The length ℓ_p is an effective capillary length.

Another restoring force is due to the bending rigidity, $B = Et^3/[12(1-\nu^2)]$. However, previous work [6, 7] has shown that the effect of bending may be neglected when the internal pressure, p, is sufficiently large. To see this, we note that the foundation stiffness resulting from bending effects $\sim B/\ell_p^4$, which is significantly smaller than the foundation stiffness $\kappa_w \sim Et/R^2$ (discussed above) when

$$\tau = \frac{pR^2}{(EtB)^{1/2}} \gg 1. \qquad (2)$$

The parameter τ may be thought of as the dimensionless pressure within the shell. Since τ is the ratio between the tension–induced and bending–induced stiffnesses of the shell, it is also similar to the "tensional bendability" introduced in recent studies of uniaxially stretched sheets [20]. We neglect the effects of bending since all simulations reported here have $\tau \gtrsim 25$. In the language of [21], we consider the limit of large bendability.

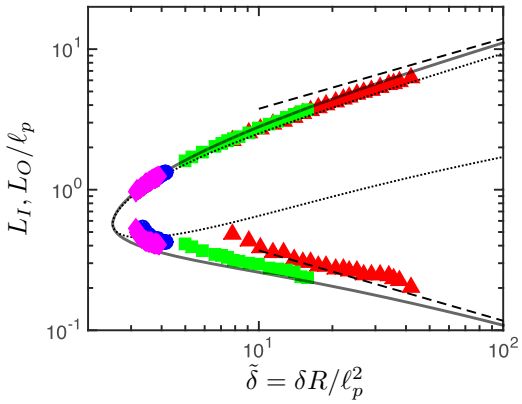

Fig. 2: The evolution of the inner and outer wrinkle positions, L_I and L_O, with increasing indentation depth $\tilde{\delta}$. The results of ABAQUS simulations are shown for different values of the dimensionless pressure τ and thickness ratio t/R: $\tau = 26.2, t/R = 3 \times 10^{-4}$ (red triangles), $\tau = 52.5, t/R = 3 \times 10^{-4}$ (green squares), $\tau = 177, t/R = 2 \times 10^{-3}$ (blue circles) and $\tau = 378, t/R = 1 \times 10^{-3}$ (magenta diamonds). The predictions of the FT membrane theory (valid as $\tau \to \infty$) are shown (solid black curve) together with the asymptotic results (10) and (13) (dashed lines). For comparison, the results of the axisymmetric membrane-shell theory [7] are also shown (dotted curve).

The picture outlined above holds while the stress within the shell remains close to its pre-indentation level. However, indentation also introduces a geometrical strain $\epsilon \sim (\delta/\ell_p)^2$, and a corresponding contribution to the stress $\sim Et\delta^2/\ell_p^2$. This additional stress leads to an inhomogeneity in the stress within the shell: the radial stress $\sigma_{rr}(r)$ decreases monotonically to the far-field value, $\sigma_\infty = pR/2$, while the hoop stress $\sigma_{\theta\theta}$ decreases more rapidly and overshoots the far-field value (since material circles are pulled inwards and become relatively compressed) [7, 22]. The relative size of the geometrical stress $\sim Et\delta^2/\ell_p^2$ and the pre-stress $\sim pR$ is a function only of the ratio:

$$\tilde{\delta} = \delta R/\ell_p^2 \;=\; Et\delta/pR^2. \qquad (3)$$

Here, this dimensionless indentation depth plays the role of the "confinement" parameter introduced in previous studies [22–24]. Above a critical value, $\tilde{\delta} > \tilde{\delta}_c \approx 2.52$, the hoop stress becomes compressive, $\sigma_{\theta\theta} < 0$, beginning a distance $r_c \approx 0.58\ell_p$ from the indenter and confined to an annulus $L_I < r < L_O$ as $\tilde{\delta}$ increases [7]. Since we assume that $\tau \gg 1$, (the shell has negligible resistance to compression), any compressive stress immediately leads to wrinkling. Assuming that the shell remains close to its axisymmetric state, detailed calculations [7] show that as $\tilde{\delta}$ increases, wrinkles are confined to an annulus $L_I < r < L_O$ with both L_I and L_O increasing (see fig. 2).

Simulations confirm the behaviour at the onset of wrinkling [7], in particular the prediction $\tilde{\delta}_c \approx 2.52$. However, as fig. 2 shows, systematic discrepancies are observed in the wrinkle position as indentation increases beyond $\tilde{\delta}_c$. In this letter, we show that this discrepancy signals an important change in the mechanical response.

Tension field theory description of wrinkling. – The key ingredient missing from previous works [6, 7] is that the hoop stress, $\sigma_{\theta\theta}$, cannot become arbitrarily large and negative. Instead, the appearance of wrinkles allows the shell to relax the compressive stress so that $\sigma_{\theta\theta} \approx 0$, a result that is referred to variously as Tension field theory [25,26], Relaxed energy [27,28] or Far from threshold (FT) wrinkling [20, 29].

An immediate consequence of the collapse of hoop stress, $\sigma_{\theta\theta} \approx 0$, is that the radial stress $\sigma_{rr} \approx C/r$ in the wrinkled region ($L_I < r < L_O$), for some constant C. We denote the normal displacement of the wrinkled shell from its natural state by $\zeta(r,\theta) = \bar{\zeta}(r) + f(r)\cos m\theta$: $\bar{\zeta}$ is the mean displacement upon which m fine wrinkles of amplitude $f(r)$ are placed. (Here r is the horizontal distance from the axis of indentation and θ the azimuthal coordinate, see fig. 1c.) In the FT approach, $\bar{\zeta}(r)$ is determined at leading order with m and f determined subsequently [20, 23]. In the wrinkled zone vertical force balance reads [30]

$$\frac{C}{r}\left(\frac{1}{R} - \frac{\mathrm{d}^2\bar{\zeta}}{\mathrm{d}r^2}\right) = p - \frac{F}{2\pi}\frac{\delta(r)}{r}, \tag{4}$$

which can immediately be integrated to give

$$\bar{\zeta} = A + \frac{r^2}{2R} - \frac{pr^3}{6C} + \frac{F}{2\pi C}r \tag{5}$$

for some constant of integration A and the force F.

To determine A, F, and C, together with the inner and outer limits of the wrinkled region, L_I and L_O, the above solution must be patched together with the solution of the vertical force balance in the tensile (i.e. unwrinkled) regions $0 \le r < L_I$ and $r > L_O$, which reads [7, 30]

$$\frac{1}{r}\frac{\mathrm{d}}{\mathrm{d}r}\left[\left(\frac{r}{R} - \frac{\mathrm{d}\zeta}{\mathrm{d}r}\right)\psi\right] = p - \frac{F}{2\pi}\frac{\delta(r)}{r}. \tag{6}$$

Here $\psi(r)$ is the Airy potential, such that $\sigma_{rr} = \psi/r$ and $\sigma_{\theta\theta} = \psi'$, which satisfies the compatibility condition [7]

$$\frac{1}{Y}r\frac{\mathrm{d}}{\mathrm{d}r}\left[\frac{1}{r}\frac{\mathrm{d}}{\mathrm{d}r}(r\psi)\right] = \frac{r}{R}\frac{\mathrm{d}\zeta}{\mathrm{d}r} - \tfrac{1}{2}\left(\frac{\mathrm{d}\zeta}{\mathrm{d}r}\right)^2. \tag{7}$$

Each of the equations in the tensile regions, (6) and (7), is second order; there are therefore 4 degrees of freedom associated with each tensile region. In the wrinkled region there are 3 degrees of freedom (A, C and F). Finally, with the radii of the wrinkled zone L_I, L_O, we have 13 degrees of freedom in total, which must match the number of boundary conditions (BCs). At the indenter, $r = 0$, we impose the vertical displacement, $\zeta(0) = -\delta$, while the radial displacement vanishes, $u_r(0) = 0$. Far from the indenter, we require that $\zeta(r) \to 0$, while $\psi \approx pRr/2$, the uniformly stressed solution. In addition, we also require continuity of ζ, ζ', σ_{rr}, $\sigma_{\theta\theta}$ and u_r, at $r = L_I$ and $r = L_O$. The first four of these continuity conditions at each boundary, together with the conditions at 0 and ∞, give a total of 12 BCs. Imposing continuity of u_r at L_I and L_O requires the integration of a further equation for $\partial u_r/\partial r$ across the wrinkled region, introducing a new unknown and two BCs. After some algebra a single condition emerges

$$\frac{C}{Y}\log\frac{L_O}{L_I} = \int_{L_I}^{L_O} \tfrac{1}{2}\left(\frac{\mathrm{d}\bar{\zeta}}{\mathrm{d}r}\right)^2 - \frac{r}{R}\frac{\mathrm{d}\bar{\zeta}}{\mathrm{d}r}\,\mathrm{d}r. \tag{8}$$

Here, the LHS and RHS represent, respectively, the stretching of lines of longitude, and how the boundary displacement differs from that expected were the shell to deform inextensibly.

Equations (5)–(8) can be solved numerically using the MATLAB multipoint boundary value problem solver `bvp4c`. For a given $\delta > \delta_c$, the solution gives the inner and outer limits of the wrinkled region (L_I and L_O respectively), together with the force F. Figure 2 shows the evolution of L_I and L_O with $\tilde{\delta}$, together with the results of our ABAQUS simulations. Also shown for comparison are the extent of the compressive hoop stress for a perfectly axisymmetric membrane-shell [7]. The agreement between simulations and the results of this collapsed-compressive stress model, which takes into account the non-perturbative effect of wrinkling on the shell shape, is significantly better than that based on the axisymmetric membrane-shell theory. In particular, we observe that L_I decreases with increasing $\tilde{\delta}$ — qualitatively different from the predictions of a standard post-buckling analysis [7].

Figure 3 shows the force–displacement relationship: ABAQUS simulations and the numerical solution of (5)–(8) produce results that are in good agreement with each other. Furthermore, in the limit of large indentation depths, the force-displacement relationship becomes linear, corresponding to a constant stiffness $k = F/pR\delta$ (inset of fig. 3). At the scaling level, this result is in qualitative agreement with prior analysis of the axisymmetric membrane-shell equations and with the simple picture of deformation being accommodated via mirror-buckling [6]: the work done $\sim F\delta$ is stored purely in the gas compressed at constant pressure $p\Delta V \sim p[(\delta R)^{1/2}]^2\delta$, so that $F \sim pR\delta$. However, for the axisymmetric, mirror-buckled shape, a detailed calculation predicts that $k = F/pR\delta = \pi$ [6] while fig. 3 indicates that $k \approx 2$. To gain quantitative understanding of the differences between the axisymmetric membrane theory and the compressed-stress approach described so far, we now consider the limit of very large indentation depths, $\tilde{\delta} \gg 1$.

Analytical results for large indentation. – As already remarked, $L_I \to 0$ as δ increases. This can be shown by a more formal calculation [30] but for now we make this an ansatz that we verify *a posteriori*. With this assumption, it is clear that the constant A in (5) is

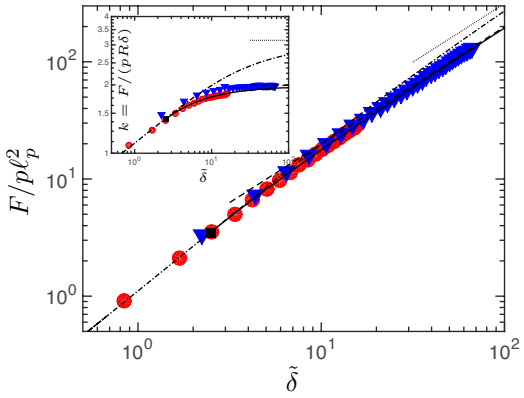

Fig. 3: Numerical results for the force–displacement relationship of an indented pressurized shell. The results of ABAQUS simulations are shown for a shell thickness $t/R = 3 \times 10^{-4}$. Different pressurisations are used: $p = 0.1$ MPa, $\tau \approx 52.5$ (red circles) and $p = 0.05$ MPa, $\tau \approx 26.2$ (blue triangles). The numerical solutions of (5)–(8) are shown (solid black curve) with the asymptotic relationship (12) (dashed black line). The corresponding results for a perfectly axisymmetric shell are also shown (dash-dotted curve) with the ultimate mirror-buckling result $F = \pi\delta pR$ (dotted line) [6]. The black square shows the onset of wrinkling, at $\tilde{\delta} \approx 2.52$.

$A \approx -\delta = \bar{\zeta}(0)$, the imposed indentation depth. A detailed calculation [30] shows that outside the wrinkled region, $r > L_O$, the vertical deflection of the shell decays exponentially. For the wrinkled zone to patch onto this we must have $\bar{\zeta}(L_O) = \bar{\zeta}'(L_O) = 0$. The deflection of the wrinkled portion of the shell may then be rewritten

$$\frac{\bar{\zeta}}{\delta} = -1 + \left(\frac{3}{2} - \frac{\lambda^2}{4}\right)\xi + \frac{\lambda^2}{2}\xi^2 - \left(2+\lambda^2\right)\xi^3/4 \qquad (9)$$

where $\xi = r/L_O$ and $\lambda = L_O/(\delta R)^{1/2}$. Substituting (9) into the constraint (8), and neglecting the logarithmic term, we find $\lambda = [6(\sqrt{5}-2)]^{1/2} \approx 1.19$ so that for $\tilde{\delta} \gg 1$:

$$L_O \approx 1.19013(\delta R)^{1/2} \qquad (10)$$

Comparing coefficients between Eqs. (9) and (5) we find:

$$C = \frac{\lambda^3}{3(1+\lambda^2/2)} p\delta^{1/2}R^{3/2} \approx 0.329 p\delta^{1/2}R^{3/2}\ , \qquad (11)$$

$$F \sim 6\pi C\delta \frac{3-\sqrt{5}}{2\lambda(\delta R)^{1/2}} \approx 1.99 pR\,\delta. \qquad (12)$$

To determine how L_I vanishes with increasing indentation depth we use a scaling argument. Recall that the radial stress in the wrinkled region is given by $\sigma_{rr} = C/r$. The stress in the inner tensile region ($r < L_I$) may be estimated by using the geometrically induced strain in the deformed region, $r < L_O$, giving $\sigma_{rr} \sim Et(\delta/L_O)^2$ (a similar estimate for the stress in a tensile inner core has been used in a related problem [22]). Equating these two stresses at the inner edge of the wrinkles, we find that $L_I \sim pR^{5/2}\delta^{-1/2}/(Et)$. A detailed calculation [30] yields:

$$\frac{L_I}{\ell_p} \approx 1.16923 \left(\frac{\ell_p^2}{\delta R}\right)^{1/2}. \qquad (13)$$

The predictions (10), (12) and (13) are in excellent agreement with the solution of the full tension-field problem and with ABAQUS simulations (figs 2 and 3).

We note that the force law in (12) has the same scaling behaviour as the perfectly axisymmetric case [6], but with prefactor 1.99 rather than π. In particular, this scaling is independent of the elastic properties of the shell (E and t) depending only on the internal pressure and shell radius. In the perfectly axisymmetric shell, this independence of material properties was a natural consequence of mirror-buckling being an isometry of the shell [6]. We shall see that an asymptotic isometry of the wrinkled shell (i.e. with the compression collapsing faster than the residual tension), underlies the form of the force law in (12).

Finally, using the various pre-factors determined by the preceding analysis, we rewite Eq. (9):

$$\frac{\bar{\zeta}}{\delta} \approx -1 + 0.963\frac{r}{(\delta R)^{1/2}} + \frac{1}{2}\frac{r^2}{\delta R} - 0.507\frac{r^3}{(\delta R)^{3/2}}, \qquad (14)$$

for $1.17\ell_p^2/(\delta R)^{1/2} \lesssim r \lesssim 1.19(\delta R)^{1/2}$. When written in this way the profile in (14) appears universal. Fig. 4 shows that cross-sections of simulated shells tend to this universal shape as the confinement $\tilde{\delta}$ increases. In particular, we see that (14) gives a much better account of numerical simulations than classic mirror-buckling, which, in this notation would read $\zeta/\delta \approx -1 + r^2/(\delta R)$. A puzzling observation is the asymmetry of wrinkle crests and troughs: the profile (14) captures the former better than the latter.

The energy stored in the indented shell. – Let us evaluate now the elastic energy stored in the shell at large indentation depth, when $L_I/\ell_p \to 0$. This energy consists of two principal parts: the stretching energy $\mathcal{U}_{\rm strain}$ stored in the tensile component $\sigma_{rr} = C/r$ of the compression-free stress field, and the bending energy $\mathcal{U}_{\rm bend}$ of the wrinkles. The evaluation of $\mathcal{U}_{\rm strain}$ is straightforward:

$$\mathcal{U}_{\rm strain} = \pi \int_{L_I}^{L_O} r\sigma_{rr}\epsilon_{rr}\ {\rm d}r \sim \frac{p^2R^3}{Et}\delta \log\tilde{\delta}\ , \qquad (15)$$

where we used Eq. (11). A more careful calculation of $\mathcal{U}_{\rm strain}$, which accounts also for the tensile core zone $r < L_I$, confirms this scaling relation.

A calculation of $\mathcal{U}_{\rm bend}$, similarly to previous works [21, 23], proceeds in two steps. First, we express the energy as a function of m only, by employing a "slaving" condition between the number, m, and amplitude, $f(r)$, of wrinkles:

$$\frac{m^2f^2}{4r} = \frac{C}{Y}\log\frac{L_O}{r} + \int_r^{L_O}{\rm d}r\left[\frac{r}{R}\frac{{\rm d}\bar{\zeta}}{{\rm d}r} - \tfrac{1}{2}\left(\frac{{\rm d}\bar{\zeta}}{{\rm d}r}\right)^2\right]. \qquad (16)$$

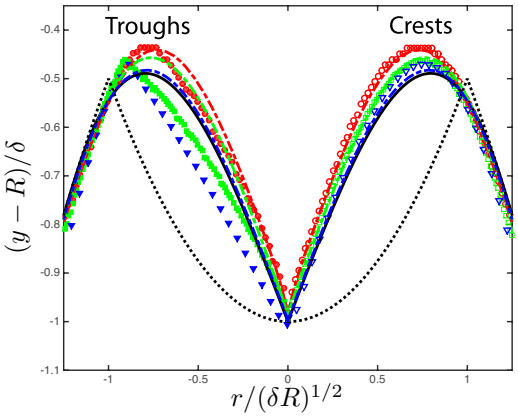

Fig. 4: Approach to the wrinkly isometry of a pressurized shell. Cross-sections through an indented pressurized shell, obtained from ABAQUS simulations, are shown for different indentation depths with $\tau \approx 52.5$: $\tilde{\delta} = 6.1$ (red circles) and $\tilde{\delta} = 15$ (green squares); to reach larger indentations numerically we must consider lower pressure, $\tau = 26.2$ and $\tilde{\delta} \approx 90.3$ (blue triangles). Cross-sections through a trough in the wrinkle pattern are shown on the left ($r < 0$); Cross-sections through a crest are shown on the right ($r > 0$). The predictions of the FT theory with the corresponding (finite) value of $\tilde{\delta}$ are shown by the coloured dash-dotted curves. As $\tilde{\delta}$ increases the deformation tends to the wrinkly isometry (14) (solid black curve), rather than the classic mirror-buckled isometry (dotted curve).

Here the RHS may be calculated from the results of the preceding analysis, Eqs. (5,10,11,12). Physically, (16) stems from the fact that, for the compressive stress to collapse, the azimuthal undulations must accommodate the excess length of deformed latitudes. (Notice also that Eq. (8) can be obtained from the slaving condition (16) since the wrinkle amplitude vanishes at $r = L_I, L_O$.)

In the second step, one determines the energetically favorable value of m, for which the bending energy balances the contribution of wrinkles to the stretching of longitudes (beyond $\mathcal{U}_{\rm strain}$). Intuitively, bending favors small curvature (i.e. small m) while stretching resists deviations from $\bar{\zeta}(r)$, thus favoring small $f(r)$ or, by condition (16), large m. The detailed calculation [30] yields:

$$m \sim \left(\frac{\tilde{\delta}^2}{\log\tilde{\delta}}\right)^{1/4} \tau^{1/2}\ , \qquad (17)$$

and gives the bending energy

$$\mathcal{U}_{\rm bend} \sim pR\delta^2(\log\tilde{\delta})^{1/2}/\tau. \qquad (18)$$

As shown above, our ABAQUS simulations are in excellent agreement with the macroscale features of the wrinkle pattern predicted theoretically (L_I, L_O, F and the shell profile). However, while close to threshold (i.e. $\tilde{\delta} = O(1)$), previous ABAQUS simulations [7] confirm the τ dependence predicted by (17), the predicted evolution of m with increasing $\tilde{\delta}$ has not been observed. This shortcoming is consistent with recent work, which showed significant hurdles in numerically predicting the wrinkle number [31]. In that study, which addressed a planar sheet under differential tensile loads, it was shown that under-damped dynamic relaxation allows "hopping" between meta-stable states, leading ultimately to the ground state (i.e. the wrinkle number of the global energy minimizer). In our simulations, the lack of variation of wrinkle number persists despite our use of an over-damped relaxation technique, suggesting either a sensitivity to numerical technique or a higher energetic barrier between meta-stable states than in other problems [31]. Additionally, a more elaborate calculation of the energy may result in a spatial profile of the wrinkle number, $m \to m(r)$ [28, 32, 33].

Wrinkly isometry. – A key feature of (14) in the limit of very large indentations, $\tilde{\delta} \gg 1$, is that the wrinkle pattern covers almost the entire region from the indenter to the outer ridge, which is positioned at $r \approx 1.19(\delta R)^{1/2}$; outside this ridge, the shell is effectively undeformed [30]. As such, the work done in compressing the gas is:

$$\mathcal{U}_{\rm gas} = p\Delta V = 2\pi p \int_{L_I}^{L_O} r\bar{\zeta}\ {\rm d}r \approx 0.995 pR\delta^2. \qquad (19)$$

Interestingly, the derivative ${\rm d}\mathcal{U}_{\rm gas}/{\rm d}\delta$ is identical to the total force F calculated above (Eq. 12). The origin of this remarkable feature is elucidated by comparing $\mathcal{U}_{\rm gas}$ to the energies of stretching and bending stored in the poked shell. We have that $\mathcal{U}_{\rm strain}/\mathcal{U}_{\rm gas} \sim (\log\tilde{\delta})/\tilde{\delta} \ll 1$, since (14) only holds for $\tilde{\delta} \gg 1$. At the same time, for the FT expansion [20] to be valid we must have $\mathcal{U}_{\rm bend} \ll \mathcal{U}_{\rm gas}$, i.e. $\tau \gg (\log\tilde{\delta})^{1/2}$. The two components of the elastic energy are therefore negligible in comparison to the work done in compressing the gas at constant pressure; this is the signature of the "asymptotic isometry" that is realized by the wrinkled shell.

Rather than a specific shape, such as mirror-buckling, which exists also in the absence of pressure, and to which the undeformed shell can be mapped isometrically almost everywhere (except at the circular ridge), a wrinkled shell develops finer and finer structure in a macroscopic zone ($L_I < r < L_O$). However, this isometric shape can only be approached when both $\mathcal{U}_{\rm bend}, \mathcal{U}_{\rm strain} \ll \mathcal{U}_{\rm gas}$, i.e. when

$$1 \ll \tilde{\delta} \ll \exp(\tau^2). \qquad (20)$$

We shall show shortly that this occurs when both the shell thickness and the pressure become asymptotically small. Such a doubly asymptotic approach to isometry has been noted recently in set-ups that involve strong deformation of thin sheets; in these systems the work done by the external load is generally stored elsewhere than the deformed sheet itself [21, 22, 34].

Conclusion. – Why is the wrinkly isometry selected by the poked shell, and not the simpler, mirror-buckled isometry? In the parameter regime (20) the deformation energy is well-approximated by $\mathcal{U}_{\rm gas}$ alone: the energies of bending and stretching (which are localized in the circular ridge of the mirror-buckled shape but spread around in

the wrinkly isometry) are insignificant. The only energy that one should compare then is the work of compressing the gas. In both types of isometric response this energy $\propto pR\delta^2$ but for wrinkly isometry the prefactor ≈ 0.995 while for mirror-buckling it is $\pi/2$: since wrinkly isometry compresses less gas than mirror-buckling, it is, in this limit, energetically favourable to mirror-buckling.

To understand the physical nature of the asymptotic parameter regime (20), we note that (20) may be re-written $1 \ll \delta/(t\tau) \ll \exp(\tau^2)$. For a fixed indentation depth δ, the first inequality may be achieved if, $t\tau \to 0$; however, the second inequality then holds only if $\tau \to \infty$. If the Young's modulus and radius of the shell are considered fixed (as in our simulations) this may be achieved with vanishing thickness and pressure, $t, p \to 0$, but with the additional requirements that $p/t \to 0$ and $p/t^2 \to \infty$ (e.g. $p \sim t^\alpha$ for any $1 < \alpha < 2$). The wrinkly isometry therefore exists if the pressure is sufficiently weak, but not too weak.

If instead, $p/t^2 \to 0$ as $t \to 0$, the pressure is "ultra-weak". In this case, the energy of deformation is not well-approximated by $\mathcal{U}_{\rm gas}$, and the bending energy of deformation must be considered. One might guess that in such a case the deformed shell will approach isometry simply by selecting the mirror buckled shape. A host of experimental and computational studies [13,14], as well as one's own experience of poking a ping-pong ball, indicate that such a guess is naive: instead, a polygonal shape is formed, with a number of vertices that increases slowly upon increasing indentation depth (relative to thickness). Such a shape is strictly different from both the axisymmetric mirror-buckled shape and the wrinkly isometry described here (for a weak, but not ultra-weak, pressure). This suggests the fascinating possibility that a new type of isometry characterizes the poked shell for small thicknesses and ultra-weak pressure. We hope that future work will clarify the nature of this third type of isometry of shells.

* * *

We thank the Aspen Center for Physics and the Parsegians' Casa Física for hospitality during this work. This research was supported by a Leverhulme Trust Research Fellowship (D.V.), the Zilkha Trust, Lincoln College (D.V.), the European Research Council under the European Horizon 2020 Programme, ERC Grant Agreement no. 637334 (D.V.), NSF-CAREER Grant No. CMMI-1149750 (H.E and A.V.), NSF-CAREER Grant No. DMR 11-51780 (B.D.) and a fellowship from the Simons Foundation, Award No. 305306, (B.D.).

REFERENCES

[1] Vaziri A., Lee H. and Kaazempur Mofrad M. R., *J. Mater. Res.* , **21** (2006) 2126.
[2] Hernando-Pérez M., Miranda R., Aznar M., Carrascosa J. L., Schaap I. A. T., Reguera D. and de Pablo P. J., *Small* , **8** (2012) 2366.
[3] Arnoldi M., Fritz M., Baüerlein E., Radmacher M., Sackmann E. and Boulbitch A., *Phys. Rev. E* , **62** (2000) 1034.
[4] Arfsten J., Leupold S., Bradtmöller C., Kampen I. and Kwade A., *Colloids Surf. B* , **79** (2010) 284.
[5] Gordon V. D., X.Chen, Hutchinson J. W., Bausch A. R., Marquez M. and Weitz D. A., *J. Am. Chem. Soc.* , **126** (2004) 14117.
[6] Vella D., Ajdari A., Vaziri A. and Boudaoud A., *J. R. Soc. Interface* , **9** (2012) 448.
[7] Vella D., Ajdari A., Vaziri A. and Boudaoud A., *Phys. Rev. Lett.* , **107** (2011) 174301.
[8] Reissner E., *J. Math. Phys.* , **25** (1947) 80.
[9] Reissner E., *J. Math. Phys.* , **25** (1947) 279.
[10] Pogorelov A. V., *Bending of Surfaces and Stability of Shells* (AMS Bookstore, Providence, RI) 1988.
[11] Audoly B. and Pomeau Y., *Elasticity and Geometry* (Oxford Univ. Press) 2010.
[12] Fitch J. R., *Int. J. Sol. Struct.* , **4** (1968) 421.
[13] Vaziri A. and Mahadevan L., *Proc. Natl. Acad. Sci. USA* , **105** (2008) 7913.
[14] Vaziri A., *Thin Wall. Struct.* , **47** (2009) 692.
[15] Nasto A., Ajdari A., , Lazarus A., Vaziri A. and Reis P. M., *Soft Matter* , **9** (2013) 6796.
[16] Nasto A. and Reis P. M., *J. Appl. Mech.* , **81** (2014) 121008.
[17] Ebrahimi H., Ajdari A., Vella D., Boudaoud A. and Vaziri A., *Phys. Rev. Lett.* , **112** (2014) 094302.
[18] Knoche S. and Kierfeld J., *EPL* , **106** (2014) 24004.
[19] Knoche S. and Kierfeld J., *Eur. Phys. J. E* , **37** (2014) 1.
[20] Davidovitch B., Schroll R. D., Vella D., Adda-Bedia M. and Cerda E., *Proc. Natl. Acad. Sci. USA* , **108** (2011) 18227.
[21] Hohlfeld E. and Davidovitch B., *Phys. Rev. E* , **91** (2015) 012407.
[22] Vella D., Huang J., Menon N., Russell T. P. and Davidovitch B., *Phys. Rev. Lett.* , **114** (2015) 014301.
[23] King H., Schroll R. D., Davidovitch B. and Menon N., *Proc. Natl. Acad. Sci. USA* , **109** (2012) 9716.
[24] Grason G. and Davidovitch B., *Proc. Natl. Acad. Sci. USA* , **110** (2013) 12893.
[25] Stein M. and Hedgepeth J. M., Tech. Rep. NASA (July 1961).
[26] Steigmann D. J., *Proc. R. Soc. A* , **429** (1990) 141.
[27] Pipkin A. C., *IMA J. Appl. Math.* , **36** (1986) 85.
[28] Bella P. and Kohn R. V., *Commun. Pure. Appl. Math.* , **67** (2014) 693.
[29] Davidovitch B., Schroll R. D. and Cerda E., *Phys. Rev. E* , **85** (2012) 066115.
[30] Vella D., Ebrahimi H., Vaziri A. and Davidovitch B., *arXiv:1508.06146* , (2015)
[31] Taylor M., Davidovitch B., Qiu Z. and K. Bertoldi, *J. Mech. Phys. Sol.* , **79** (2015) 92.
[32] Piñeirua M., Tanaka N., Roman B. and Bico J., *Soft Matter* , **9** (2013) 10985.
[33] Paulsen J. *et al.*, *In Preparation*, (2015) .
[34] Chopin J., Démery V. and Davidovitch B., *J. Elast.* , **119** (2015) 137.